Metabolic and behavioral alterations associated with viral vector-mediated toxicity in the paraventricular hypothalamic nucleus

Rohan Savani[1,2], Erin Park[1,2], Nidhi Busannagari[1,2], Yi Lu[1], Hyook Joon Kwon[3], Le Wang[1, *], Zhiping P. Pang[1, *]

[1]The Child Health Institute of New Jersey, Robert Wood Johnson Medical School, Rutgers, The State University of New Jersey, New Brunswick, NJ, USA
[2]Department of Cell Biology and Neuroscience, Undergraduate Program, Rutgers, The State University of New Jersey, New Brunswick, NJ, USA
[3]Department of Medicine, Rutgers-Robert Wood Johnson Medical School, New Brunswick, NJ, 08901, USA

Main text Words: 3467

Figures: 3

*Corresponding authors:

Le Wang: lw611@rwjms.rutgers.edu

Zhiping P. Pang: pangzh@rwjms.rutgers.edu

ABSTRACT

Objective: Combining adeno-associated virus (AAV)-mediated expression of Cre recombinase with genetically modified floxed animals is a powerful approach for assaying the functional role of genes in regulating behavior and metabolism. Extensive research in diverse cell types and tissues using AAV-Cre exemplifies advantages over crossing with Cre driver lines in several aspects, including saving time and avoiding developmental/compensatory issues. We initially sought to study the impact of ablation of corticotropin-releasing hormone (CRH) in the paraventricular hypothalamic nucleus (PVN) using intracranial AAV8-hSyn-Cre injection in adult animals.

Methods: In this study, we stereotactically injected AAV8-hSyn-Cre or a control viral vector (1E13 and 1E12 vg/ml, respectively, both at 150 nL) in both Crh-floxed and wild-type mouse PVN to assess behavioral and metabolic impacts. We then used immunohistochemical markers to systematically evaluate the density of hypothalamic peptidergic neurons and glial cells.

Results: We found that delivery of one preparation of AAV8-hSyn-Cre in the PVN led to the development of obesity, hyperphagia, and anxiety-like behaviors. This effect occurred independent of sex and in both floxed and wild-type mice. We subsequently found that AAV8-hSyn-Cre led to neuronal cell death and gliosis at the site of viral vector injections. These behavioral and metabolic deficits were dependent on injection into the PVN specifically.

Conclusions: Our findings reveal that delivery of AAV8-hSyn-Cre could lead to cellular toxicity and lesions in the PVN that cause robust metabolic and behavioral impacts. These alterations can complicate the interpretation of AAV-Cre-mediated gene knockout and highlight the need for rigorous controls.

Keywords: AAV, toxicity, paraventricular hypothalamus, obesity

1. INTRODUCTION

Located in the ventral forebrain, the paraventricular nucleus of the hypothalamus (PVN) acts as a major integrative center for diverse regulatory functions, including neuroendocrine response, autonomic tone, and complex behaviors including food intake and social interaction (1-3). Dissecting the molecular, morphological, and functional heterogeneity of the PVN has thus far given rise to several distinct cell types involved in the control of these processes.

Refining our understanding of how the PVN integrates and outputs multimodal information across neuroendocrine and autonomic pathways may inform several disorders, including cardiovascular, metabolic, and neuropsychiatric disorders (2, 4, 5). However, the PVN contains spatially intermingled but functionally distinct populations that can only be selectively targeted through genetic access, such as conditional knockout (KO) by Cre-lox recombination (6, 7). While much work relies on promoter-driven Cre expression, another standard method relies on adeno-associated virus-mediated Cre expression (AAV-Cre) (8-11). Methods such as AAV-mediated Cre delivery in adult mice are valuable approaches to bypass transient developmental transcription and ensure high-fidelity expression in specific brain regions (8, 12). However, emerging evidence suggests that there may be deleterious effects associated with AAV-Cre, resulting in morphological and behavioral abnormalities even in the absence of loxP sequences (13, 14).

In this study, we assessed the striking phenotype that emerged from the delivery of an AAV-Cre-prepared virus in the PVN of adult *Crh-flox* (*Crh*$^{f/f}$) mice. We found that *Crh*$^{f/f}$ mice with putatively knocked out corticotropin-releasing hormone (CRH) via AAV-mediated expression of Cre recombinase in the PVN rapidly developed obesity and metabolic syndrome, which was an intriguing and unexpected finding. However, subsequent rigorous analysis revealed that both CRH- and oxytocin-expressing neuron densities significantly decreased, likely due to cellular toxicity at the injection sites. Our study confirms the importance of the PVN in the control of metabolism and highlights the potential for toxicity due to a commonly used AAV, which necessitates careful interpretation and proper controls for experiments utilizing viral vectors.

2. MATERIALS AND METHODS

2.1 Animals

All studies and procedures involving mice were approved by the Rutgers University Institutional Animal Care and Use Committee (IACUC) and by the National Institute of Health (NIH) guidelines. The animals used in this study were 5-7 weeks old at the time of stereotactic surgery. *Crh*$^{f/f}$ mice

77 (15), *Glp1r*$^{f/f}$ mice (16), and wild-type (C57BL/6) mice were used in this study. For each
78 experimental paradigm, littermate mice were randomized to each experimental group on the basis
79 of body weight. Both males and females were used in this study. Mice of both groups were housed
80 together. Investigators were blinded to treatment. The sample size required (n=5-7) for each group
81 was estimated from previous studies (17).

82 ***2.2 AAV vectors and stereotactic surgery***

83 The AAVs used in this study included pAAV-hSyn-EGFP (Addgene, #50465-AAV8, titer: titer
84 7×10^{12} vg/mL) and pENN.AAV.hSyn.HI. eGFP-Cre.WPRE.SV40 (Addgene, #105540-AAV8, titer:
85 $1\text{x}10^{13}$ vg/mL). For surgical injections, mice were anesthetized with isoflurane and placed in a
86 stereotactic frame. Burr holes were drilled above the injection sites. 150 nL of the viruses were
87 bilaterally stereotactically injected in the PVN (AP: -0.7, ML: ±0.18, DV: -4.7) at a rate of 1 nL/s
88 (eGFP for control group, Cre for experimental group). For experiments in the dorsolateral septum
89 (dLS), 100 nL of viruses were bilaterally injected in the dLS (AP: +0.5, ML: ±0.45, DV: -2.7) at a
90 rate of 1 nL/second. Mice recovered for at least 3 weeks prior to conducting behavioral
91 experiments. Injection sites were confirmed by *post hoc* histological examinations.

92 ***2.3 Metabolic phenotyping***

93 All experiments were conducted during the light cycle unless otherwise stated. Investigators were
94 blinded to conditions during experiments.

95 *Plasma corticosterone measurements*: Blood was collected either at the beginning of the ITT test
96 or during transcardiac perfusion. At least 10 µL was collected into EDTA-coated tubes and then
97 centrifuged at 8000rpm at 4°C for 5 minutes. Extracted plasma was stored at -80° C until further
98 processing. Corticosterone measurements were obtained with an ELISA as per manufacturer's
99 instructions (Enzo Life Sciences, ADI-900-097).

100 *Food intake*: Mice were singly housed before the experiment with ad libitum access to normal
101 chow (Purina Mouse Diet 5058) and water. Chow remaining in the cage after each day (12 hr.
102 light/dark cycle) was measured for 5 days and averaged together.

103 *EchoMRI/fat mass measurements*: Whole body composition and fat mass was measured by
104 EchoMRI (Echo Medical Systems, Houston, Texas).

105 *Comprehensive Lab Animal Monitoring System (CLAMS) assays*: *Crh*$^{f/f}$ mice were placed into
106 metabolic phenotyping cages (Columbus Instruments, OH, USA). Data was recorded every 15

107 minutes. Data was collected for 3 days (both light and dark cycles) after 2 days of habituation to
108 single housing within the cages.

109 *Glucose tolerance test (GTT) and insulin tolerance test (ITT)*: Mice were fasted overnight (GTT)
110 or for 6 hours (ITT). To minimize stress, 0.5 grams of chow was provided. For GTT, mice were
111 intraperitoneally (IP) administered 20% glucose. Blood glucose measurements were collected at
112 the 0, 15-, 30-, 60-, and 120-minute time points. For ITT, mice were IP-administered insulin.
113 Injection volumes were 0.1 mL/10 g body weight. Blood glucose measurements were collected at
114 the 0-, 15-, 30-, and 60-minute time points.

115 ***2.4 Behavioral assays***

116 *Open field test*: Mice were placed in the middle of a custom-made 45 x 45 cm square open field
117 arena for 10 minutes. Analysis was performed using DeepLabCut v2.2 (18). We labeled 150-200
118 frames taken from 14 or 10 videos, as resolution changed between recording sessions (95% of
119 frames were used for training, 5% for testing). We used a ResNet50-based network with default
120 parameters for 225,000 or 450,000 training iterations (until loss plateaued). After analyzing open-
121 field videos, we then calculated the time spent in the inner zone (inner 3/5 of the arena, ~25x25cm)
122 using a region of interest tool. Distance traveled was calculated with custom codes. Investigators
123 were blinded to the condition during analysis.

124 *Light-dark box test*: Mice were placed in the SmartCage system (AfaSci) light side of a commercial
125 light-dark box apparatus consisting of one dark and one illuminated compartment connected by
126 a door. Time spent in each zone, latency to enter the dark zone, and number of entries were
127 measured for 10 minutes. Data were analyzed using Excel.

128 ***2.5 Histology and immunohistochemistry (IHC) analysis***

129 Mice used for IHC analysis of CRH and oxytocin (OXT) were intracerebroventricularly
130 administered colchicine a day prior to perfusion. Mice were anesthetized with isoflurane and
131 perfused with PBS (pH 7.4) and then 4% paraformaldehyde (PFA). Coronal brain slices were
132 cryosectioned (50 μm). For IHC analyses, brain slices were first incubated in blocking buffer (4%
133 BSA, 1% goat serum in PBS) for 1 hour, then in primary antibody overnight at 4°C. Slices were
134 washed with blocking buffer 3x15 min prior to incubation with a secondary antibody at RT for 2
135 hours, followed by further washing with PBS. Sections were mounted with Fluoroshield with DAPI
136 (Sigma-Aldrich, # F6057). Images were collected with a Zeiss LSM700 confocal microscope. A Z-
137 stack captured the entire thickness of the section with fluorescence. NeuN-stained slices were

138 imaged at a 5 μm-thickness interval for a total range of 25 μm. Imaging analysis was performed
139 using NIH-ImageJ and with the Allen Brain Atlas as a reference. The number of OXT- and CRH-
140 cells in the PVN was counted with the Cell Counter plugin. To quantify NeuN density, images were
141 background subtracted (20-pixel radius) before converting to a binary image. Then, segmented
142 particles were filtered by despeckling twice and watershed transforming, followed by final counting
143 (minimum size of 7 μm^2). GFAP and Iba1 fluorescence area was calculated by dividing the area
144 of thresholded signal by total PVN area. The quantifications were performed by two independent
145 investigators who were blinded to the condition during analysis.

146 ***2.6: Antibodies***

147 The primary antibodies used in this study were rabbit Anti-CRH (1:500, BMA Biomedicals, #T-
148 4037, RRID: AB_2314240), mouse Anti-OXT (1:500 Sigma-Aldrich, #MABN844), rabbit Anti-
149 NeuN (1:500, Millipore, #ABN78, RRID: AB_10807945), rabbit Anti-GFAP (1:1000, Dako, #Z0334,
150 RRID: AB_10013382), and chicken Anti-Iba1 (1:500, Aves Labs, #IBA1-0020).

151 ***2.7 Statistical analysis***

152 Statistical analyses were performed using GraphPad Prism 9. Data were analyzed using
153 Student's two-tailed t-tests and two-way ANOVA followed by Bonferroni's multiple comparisons
154 tests. Data are presented as mean ± SEM. A p-value < 0.05 was considered statistically
155 significant.

156 **3. RESULTS**

157 ***3.1 Delivery of AAV-mediated Cre in the PVN rapidly induces behavioral changes and***
158 ***metabolic syndrome in Crh$^{f/f}$ animals.***

159 Our initial goal was to apprise the functional role of CRH by knocking it out in the PVN in adult
160 animals. To this end, we bilaterally stereotactically injected AAV8-hSyn-eGFP-Cre in the PVN of
161 5-7-week-old *Crh$^{f/f}$* mice, with AAV-hSyn-eGFP (Control) injected in littermate controls (**Fig. 1A**).
162 After four weeks of recovery, we found that plasma corticosterone levels in Cre-injected *Crh$^{f/f}$* mice
163 were markedly reduced, which was highly suggestive of possible loss of function of CRH (**Fig.**
164 **1B**). Even with normal chow feeding, the Cre-injected mice showed robust and rapid body weight
165 gain within days. Cre-injected mice reached an average of 50.5 ± 0.7 grams in 6 weeks, while the
166 average body weight of control animals was 28.2 ± 0.7 grams (**Fig. 1C**). The increased body
167 weight in the Cre-injected group might be, at least in part, due to elevated food intake (**Fig. 1D**).
168 We repeated these experiments in an independent cohort of *Crh$^{f/f}$* female mice (**Fig. S1A**). In this,

169 the Cre-injected group fed with normal chow weighed 45.2 ± 4.2 grams 6 weeks after viral injection
170 (**Fig. S1B**), indicating that the changes observed thus far occur in a sex-independent manner.

171 As PVN-derived CRH is known to be involved in stress-related behaviors, coping, and relief (19-
172 22), we hypothesized that reduced CRH release and corticosterone levels (**Fig. 1B**) in the Cre-
173 injected animals would be anxiolytic. To test this hypothesis, we examined anxiety-like behavior
174 in AAV-Cre injected *Crh*$^{f/f}$ male mice in the open-field and light-dark box assays (**Fig. S2**). Contrary
175 to what we hypothesized, we found that the Cre-injected mice spent less time in the center zone
176 in the open-field assay (**Fig. S2B**), and they spent more time in the dark zone during the light-
177 dark box test (**Fig. S2D**). These tests suggested that AAV-Cre in the adult PVN may lead to
178 heightened anxiety-like behaviors.

179 Nevertheless, the drastic increase in body weight of AAV-Cre-injected animals prompted us to
180 further assess their metabolic phenotype. We used CLAMS to measure energy intake and
181 expenditure, as well as to identify any changes in nutrient utilization. Compared to AAV-GFP-
182 injected animals, AAV-Cre-injected mice consumed less oxygen throughout the entire day (**Fig.**
183 **1E-F**). The respiratory exchange ratio was equal between both groups, indicating no shift in
184 nutrient utilization accompanying increases in weight (**Fig. 1G**). Energy expenditure was
185 significantly decreased in AAV-Cre-injected mice in both light and dark cycles (**Fig. 1H**). This may
186 be in part due to a decrease in locomotor activity (**Fig. 1I**). These data suggest that alterations in
187 energy expenditure may contribute to the development of obesity alongside hyperphagia in AAV-
188 Cre-injected mice. Consistent with these findings, Cre-injected mice display significantly
189 increased body fat composition (**Fig. 1J**) and significantly increased fasting plasma glucose levels
190 measured (**Fig. 1K**). To evaluate any changes in glucose and insulin homeostasis, we also
191 performed GTT and ITT. GTT revealed that Cre-injected mice had consistently elevated glucose
192 levels, indicative of higher glucose tolerance (**Fig. 1L**), while ITT revealed that they had insulin
193 resistance (**Fig. 1M**). These results indicate that Cre recombinase expression in the PVN region
194 of *Crh*$^{f/f}$ mice leads to obesity development and maintenance through changes in food intake
195 behavior and energy expenditure and causes metabolic syndrome resembling type 2 diabetes
196 mellitus.

197 Having observed the development of type 2 diabetes and obesity in the PVN Cre-injected *Crh*$^{f/f}$
198 mice, we sought to validate these findings as attributable to the depletion of hypothalamic CRH.
199 We examined CRH expression using immunohistochemistry and found decreased CRH-positive
200 cell density in the PVN of AAV-Cre-injected mice (**Fig. 2A & 2C**). This suggested that CRH

201 expression was suppressed, which supports the hypothesis that PVN CRH participates in
202 regulating metabolism. However, this hypothesis is complicated by the observation of decreased
203 OXT expression in brain sections of the same animals with Cre injections (**Fig. 2B & 2D**).
204 Decreased expression of both CRH and OXT was accompanied with a trend toward reduced cell
205 density as measured by DAPI staining (**Fig. 2E**). Based on these data, we caution that virally
206 expressed Cre recombinase may be sufficient to deplete CRH from the PVN of *Crh*$^{f/f}$ animals but
207 may also have an off-target impact on PVN neuronal cells.

208 ***3.2 Delivery of AAV-mediated Cre in the PVN rapidly alters behavior and causes metabolic***
209 ***syndrome in wild-type animals.***

210 While OXT expression may have decreased due to the development of obesity, the trend of
211 decreased cell density in the AAV-Cre group led us to hypothesize that the AAV-Cre virus may
212 impact PVN neuronal survival. The toxicity of Cre expression on cellular health has been reported
213 previously (13, 14, 23, 24).

214 To this end, we examined the impacts of AAV-Cre in C57BL/6 wild-type (WT) mice (**Fig. 3A**).
215 Similar to the AAV-Cre injected *Crh*$^{f/f}$ animals, we found a marked reduction in plasma
216 corticosterone levels in WT mice injected with AAV-Cre (**Fig. 3B**). They also gained significant
217 body weight potentially due to hyperphagia (**Fig. 3C-D**). Given that our observations closely
218 mirrored those found in *Crh*$^{f/f}$ mice, we also assessed changes in anxiety-like behaviors (**Fig. S3A**
219 **& S3C**). AAV-Cre-injected mice spent less time in the center zone during the open field test (**Fig.**
220 **S3B**). Consistent with this, Cre mice spent more time in the dark zone of the light-dark box (**Fig.**
221 **S3D**). These data suggest that the behavioral, metabolic, and cellular alterations observed with
222 Cre injection in the PVN may be due to the expression of the Cre-encoding viral vector.

223 We next systematically evaluated the number of neurons in the PVN of WT mice following AAV-
224 Cre or AAV-GFP injections using neuronal nuclei (NeuN) staining (**Fig. 3E**). Expression of NeuN
225 was significantly decreased across most of the PVN with the administration of AAV-Cre, likely due
226 to diffusion (**Fig. 3F**). Again, accompanied by the enlarged visual appearance of the third ventricle,
227 the widespread decline in neuronal density in AAV-Cre-expressing mice lends support to the idea
228 of toxic and nonspecific AAV-Cre action, resembling the effects of a chemical lesion for PVN
229 neuronal cells (25, 26). This neuronal cell loss is accompanied by astrogliosis and microglial cell
230 activation (**Fig. 3G-I**).

231 Together, these data suggest that AAV-Cre injection may cause non-specific cell death at the
232 injection site, with PVN neuronal ablation causing obesity and type 2 diabetes. This is consistent
233 with previous reports that PVN lesions result in severe obesity and dysregulated metabolism (25-
234 29).

235 ***3.3 Delivery of AAV-mediated Cre in the dorsolateral septum induces neuronal cell lesions***
236 ***without causing metabolic syndrome in Glp1r $^{f/f}$ animals.***
237 To further confirm the apparent toxicity of the AAV-Cre that we used, we tested it in another brain
238 region: the dorsal lateral septum (dLS). The glucagon-like peptide-1 receptor (GLP-1R) is highly
239 expressed in dLS and is implicated in feeding and metabolism (30-33). We assessed if a diluted
240 AAV-Cre could be used to determine endogenous GLP-1R function. To prevent the possibility of
241 cellular toxicity due to high AAV titers, we diluted our AAV to 5 x 10^{12} vg/mL and only injected 100
242 nL. We injected this AAV-Cre or a control vector in *Glp1r $^{f/f}$* mouse dLS (**Fig S4A**), but we did not
243 observe significant changes in body weight or metabolism within 4 weeks of injection (**Fig S4B**).
244 However, we found significantly decreased NeuN positive cell density (**Fig S4C-D**), suggesting
245 that Cre viral vector injection in the mouse brain causes neuronal cell loss.

246 **4. DISCUSSION**

247 In this study, we showed that delivery of one preparation of AAV-Cre recombinase in the PVN of
248 adult mice can lead to the development of metabolic syndrome and alterations in food-related and
249 anxiety-like behaviors, as well as metabolic phenotype. We demonstrated that *Crh$^{f/f}$* mice
250 expressing AAV-Cre in PVN develop obesity largely mediated by hyperphagia and changes in
251 energy expenditure. Moreover, this develops alongside glucose tolerance and insulin resistance,
252 as well as decreased locomotion. We investigated whether CRH was truly and specifically
253 depleted and found off-target effects on OXT expression (**Fig. 2**) and cell loss at sites of Cre viral
254 vector injections in either *Crh$^{f/f}$* or WT mice. These data suggested off-target effects of our viral
255 vector and indicate that caution should be used when interpreting the physiological consequences
256 of AAV injection in adult animals.

257 Specific depletion of PVN-derived CRH has thus far not been shown to induce massive metabolic
258 dysregulation when knocked out using Cre expression driven by either *Crh$^{f/f}$* crossed with *Sim1-*
259 *Cre* mice or CRISPR (17, 34). Our initial goal was to assess the impact of ablation of PVN CRH
260 in adult animals by using stereotactic injection of AAV-Cre. We observed massive obesity and
261 metabolic syndromes that starkly differ from other models of CRH knockout (17, 34-38). Despite

262 the observation of reduction of CRH expression and plasma corticosterone levels, which may be
263 an indication of impaired regulation of the hypothalamic-pituitary-adrenal axis (HPA), we surmise
264 that any metabolic or behavioral deficits reflected off-target effects of AAV-Cre. Indeed, we
265 confirmed that neuronal cell death and reactive gliosis occurred in the PVN with AAV-Cre
266 expression, resembling a response to central nervous system injury. Therefore, the study cannot
267 conclude whether adult ablation of CRH in the PVN leads to metabolic or behavioral changes in
268 adult animals.

269 The PVN is speculated to provide top-down control of feeding-related information processing via
270 intrahypothalamic connections or dense projections to midbrain and hindbrain regions (2). These
271 results could not provide insights on CRH impact on metabolism but highlight the necessity of the
272 PVN in regulating energy homeostasis and body weight. These findings are in accord with prior
273 ablation experiments and more recent work on genetic knockout models specific to the PVN (25,
274 26). It has been shown that unilateral PVH electrolytic lesions would increase lipid accumulation
275 in white adipose tissue ipsilateral to the side of the PVH (39). Chronically inhibiting PVN
276 MC4R/PDYN neuron synaptic release by expressing tetanus toxin or ablating those neurons by
277 expressing caspase-3 resulted in pronounced hyperphagia, obesity, and a significant elevation in
278 food consumption (26). Our metabolic phenotyping data revealed that cellular lesions of PVN
279 develop a strong obesity phenotype largely mediated by hyperphagia and changes in energy
280 expenditure. Moreover, dysfunction of the PVN induces hypersomnia and mediates the diurnal
281 rhythm of metabolism in mice (40, 41). Consistent with this, we also found that changes in energy
282 expenditure were more pronounced in AAV-Cre-injected mice during dark cycles (**Fig. 1H**).

283 Manipulating gene expression on and off using AAVs in genetically engineered animals is one of
284 the most powerful tools to bypass transient developmental transcription for studying gene function
285 *in vivo* (8, 12). For example, it has been shown that knockout of *Glp1r* via AAV-Cre in PVN
286 demonstrated a significant obesity phenotype, which was not observed in *Glp1r*$^{f/f}$ mice cross with
287 SIM1- or NKX2.1-Cre mice (8, 42). Similarly, AAV-CRISPR–Cas9-mediated ablation of leptin
288 receptor in arcuate nucleus demonstrated that agouti-related peptide (AgRP) neurons but not
289 proopiomelanocortin (POMC) neurons are required for the primary action of leptin to regulate both
290 energy balance and glucose homeostasis (12). The present results add to a growing body of
291 literature suggesting that toxicity occurs irrespective of serotype and brain region, though a
292 systematic comparison is lacking. Moreover, this effect may occur independent of the specific
293 virus used; while we used one viral preparation in this study, previous studies have reported
294 varying levels of success with this AAV-Cre and others (9, 13, 14, 41, 43). In the mesolimbic

295 reward system, it has been reported that Cre expression in the ventral tegmental area and
296 substantia nigra can induce toxicity associated with perturbations of dopamine-related behaviors
297 (13, 14). Further work delineating different viral preparations and optimal titers for neuronal
298 manipulations will be needed. Inducible systems of Cre expression, such as those using
299 tamoxifen, offer an appealing alternative to constitutively expressed Cre systems; however,
300 administration of tamoxifen has also been reported to lead to cytotoxicity and off-target effects
301 (44).

302 Our data confirm that the PVN is an important brain region in the regulation of metabolism;
303 dysfunction of the PVN, such as via neuronal death, causes obesity and type 2 diabetes. We also
304 conclude that AAV-Cre vector toxicity ablates PVN neurons and results in a phenotype that is not
305 associated with the gene of interest. These results underscore the importance of rigorous controls
306 to ensure virus quality and fidelity of action. Caution must especially be exercised when the
307 observed phenotype closely matches that of lesions in the area of use. Ensuring that expression
308 in wild-type mice results in no observable changes or that neuronal cell densities are unaltered (if
309 they are not expected to be) are two such methods of validating that the AAV is not toxic on its
310 own. Together, viral vectors represent a class of worthwhile tools to manipulate the nervous
311 system; however, scientists must take care to ensure that the potential for toxicity in commonly
312 used AAVs is ruled out in experimental design and data interpretation.

AUTHOR CONTRIBUTIONS

R.S. conducted animal behavior assays, histology, and data analysis. E.P. helped with histology and imaging analysis. N.B. helped with histology and imaging analysis. Y.L. conducted stereotactic surgeries, animal behavior analysis, and histology. H.J.K. conducted CLAMS experiments and corresponding data analysis. L.W. conducted stereotactic surgeries. L.W. and Z.P.P. conceived the project, and designed the experiments and wrote the paper with R.S. with input from all authors.

ACKNOWLEDGMENTS

This study was supported by grants from the Robert Wood Johnson Foundation to the Child Health Institute of New Jersey (RWJF grant #74260), and the NIH NIDDK R01DK131452. L.W. was supported by the New Jersey Governor's Council for Medical Research and Treatment of Autism Postdoctoral Fellowship (CAUT24DFP) and the NExT-Metabolism Pilot Award (500301). R.S. was supported by Rutgers Aresty Research Center's independent research award. The authors would like to thank Dr. Mark Rossi (Rutgers University) for critical reading of the manuscript and insightful comments. The graphical abstract was created with BioRender.

DATA AVAILABILITY

Code used to analyze open field test data can be found at https://github.com/RohanSavani/OpenFieldAnalysis. The data from the current study are available from the corresponding authors upon reasonable request.

SUPPLEMENTARY DATA

Supplementary data to this article: Supplemental Figures S1-S4

334 **REFERENCES**

335 1. Ferguson AV, Latchford KJ, Samson WK. The paraventricular nucleus of the hypothalamus -
336 a potential target for integrative treatment of autonomic dysfunction. Expert Opin Ther Targets.
337 2008;12(6):717-27.

338 2. Watts AG, Kanoski SE, Sanchez-Watts G, Langhans W. The physiological control of eating:
339 signals, neurons, and networks. Physiological Reviews. 2021;102(2):689-813.

340 3. Qin C, Li J, Tang K. The Paraventricular Nucleus of the Hypothalamus: Development,
341 Function, and Human Diseases. Endocrinology. 2018;159(9):3458-72.

342 4. Manaye KF, Lei DL, Tizabi Y, Dávila-García MI, Mouton PR, Kelly PH. Selective neuron loss
343 in the paraventricular nucleus of hypothalamus in patients suffering from major depression and
344 bipolar disorder. J Neuropathol Exp Neurol. 2005;64(3):224-9.

345 5. Benarroch EE. Paraventricular nucleus, stress response, and cardiovascular disease. Clinical
346 Autonomic Research. 2005;15(4):254-63.

347 6. Sauer B, Henderson N. Site-specific DNA recombination in mammalian cells by the Cre
348 recombinase of bacteriophage P1. Proceedings of the National Academy of Sciences.
349 1988;85(14):5166-70.

350 7. Tsien JZ, Chen DF, Gerber D, Tom C, Mercer EH, Anderson DJ, et al. Subregion- and Cell
351 Type–Restricted Gene Knockout in Mouse Brain. Cell. 1996;87(7):1317-26.

352 8. Liu J, Conde K, Zhang P, Lilascharoen V, Xu Z, Lim BK, et al. Enhanced AMPA Receptor
353 Trafficking Mediates the Anorexigenic Effect of Endogenous Glucagon-like Peptide-1 in the
354 Paraventricular Hypothalamus. Neuron. 2017;96(4):897-909.e5.

355 9. Deng Y, Dickey JE, Saito K, Deng G, Singh U, Jiang J, et al. Elucidating the role of Rgs2
356 expression in the PVN for metabolic homeostasis in mice. Mol Metab. 2022;66:101622.

357 10. Souza LAC, Worker CJ, Li W, Trebak F, Watkins T, Gayban AJB, et al. (Pro)renin receptor
358 knockdown in the paraventricular nucleus of the hypothalamus attenuates hypertension
359 development and AT(1) receptor-mediated calcium events. Am J Physiol Heart Circ Physiol.
360 2019;316(6):H1389-h405.

361 11. Xia H, de Queiroz TM, Sriramula S, Feng Y, Johnson T, Mungrue IN, et al. Brain ACE2
362 overexpression reduces DOCA-salt hypertension independently of endoplasmic reticulum
363 stress. Am J Physiol Regul Integr Comp Physiol. 2015;308(5):R370-8.

364 12. Xu J, Bartolome CL, Low CS, Yi X, Chien C-H, Wang P, et al. Genetic identification of leptin
365 neural circuits in energy and glucose homeostases. Nature. 2018;556(7702):505-9.

366 13. Erben L, Welday JP, Murphy R, Buonanno A. Toxic and Phenotypic Effects of AAV_Cre
367 Used to Transduce Mesencephalic Dopaminergic Neurons. Int J Mol Sci. 2022;23(16).

368 14. Rezai Amin S, Gruszczynski C, Guiard BP, Callebert J, Launay J-M, Louis F, et al. Viral
369 vector-mediated Cre recombinase expression in substantia nigra induces lesions of the
370 nigrostriatal pathway associated with perturbations of dopamine-related behaviors and
371 hallmarks of programmed cell death. Journal of Neurochemistry. 2019;150(3):330-40.

372 15. Sanford CA, Soden ME, Baird MA, Miller SM, Schulkin J, Palmiter RD, et al. A Central
373 Amygdala CRF Circuit Facilitates Learning about Weak Threats. Neuron. 2017;93(1):164-78.

374 16. Sisley S, Gutierrez-Aguilar R, Scott M, D'Alessio DA, Sandoval DA, Seeley RJ. Neuronal
375 GLP1R mediates liraglutide's anorectic but not glucose-lowering effect. The Journal of Clinical
376 Investigation. 2014;124(6):2456-63.

377 17. Zhang R, Asai M, Mahoney CE, Joachim M, Shen Y, Gunner G, et al. Loss of hypothalamic
378 corticotropin-releasing hormone markedly reduces anxiety behaviors in mice. Molecular
379 Psychiatry. 2017;22(5):733-44.

380 18. Nath T, Mathis A, Chen AC, Patel A, Bethge M, Mathis MW. Using DeepLabCut for 3D
381 markerless pose estimation across species and behaviors. Nature Protocols. 2019;14(7):2152-
382 76.

383 19. Daviu N, Bruchas MR, Moghaddam B, Sandi C, Beyeler A. Neurobiological links between
384 stress and anxiety. Neurobiology of Stress. 2019;11:100191.

385 20. Sterley T-L, Baimoukhametova D, Füzesi T, Zurek AA, Daviu N, Rasiah NP, et al. Social
386 transmission and buffering of synaptic changes after stress. Nature Neuroscience.
387 2018;21(3):393-403.

388 21. Yuan Y, Wu W, Chen M, Cai F, Fan C, Shen W, et al. Reward Inhibits Paraventricular CRH
389 Neurons to Relieve Stress. Curr Biol. 2019;29(7):1243-51.e4.

390 22. Füzesi T, Daviu N, Wamsteeker Cusulin JI, Bonin RP, Bains JS. Hypothalamic CRH neurons
391 orchestrate complex behaviours after stress. Nat Commun. 2016;7:11937.

392 23. Semprini S, Troup TJ, Kotelevtseva N, King K, Davis JR, Mullins LJ, et al. Cryptic loxP sites
393 in mammalian genomes: genome-wide distribution and relevance for the efficiency of BAC/PAC
394 recombineering techniques. Nucleic Acids Res. 2007;35(5):1402-10.

395 24. Correa-da-Silva F, Kalsbeek MJ, Gadella FS, Oppersma J, Jiang W, Wolff SEC, et al.
396 Reduction of oxytocin-containing neurons and enhanced glymphatic activity in the hypothalamic
397 paraventricular nucleus of patients with type 2 diabetes mellitus. Acta Neuropathologica
398 Communications. 2023;11(1):107.

399 25. Sims JS, Lorden JF. Effect of paraventricular nucleus lesions on body weight, food intake
400 and insulin levels. Behavioural Brain Research. 1986;22(3):265-81.

401 26. Li MM, Madara JC, Steger JS, Krashes MJ, Balthasar N, Campbell JN, et al. The
402 Paraventricular Hypothalamus Regulates Satiety and Prevents Obesity via Two Genetically
403 Distinct Circuits. Neuron. 2019;102(3):653-67.e6.

404 27. Leibowitz SF, Hammer NJ, Chang K. Hypothalamic paraventricular nucleus lesions produce
405 overeating and obesity in the rat. Physiology & Behavior. 1981;27(6):1031-40.

406 28. Fukushima M, Tokunaga K, Lupien J, Kemnitz JW, Bray GA. Dynamic and static phases of
407 obesity following lesions in PVN and VMH. American Journal of Physiology-Regulatory,
408 Integrative and Comparative Physiology. 1987;253(3):R523-R9.

409 29. Gold RM, Jones AP, Sawchenko PE, Kapatos G. Paraventricular area: Critical focus of a
410 longitudinal neurocircuitry mediating food intake. Physiology & Behavior. 1977;18(6):1111-9.

411 30. Terrill SJ, Jackson CM, Greene HE, Lilly N, Maske CB, Vallejo S, et al. Role of lateral
412 septum glucagon-like peptide 1 receptors in food intake. Am J Physiol Regul Integr Comp
413 Physiol. 2016;311(1):R124-32.

414 31. Rizzi-Wise CA, Wang DV. Putting Together Pieces of the Lateral Septum: Multifaceted
415 Functions and Its Neural Pathways. eNeuro. 2021;8(6).

416 32. Bales MB, Centanni SW, Luchsinger JR, Fathi P, Biddinger JE, Le TDV, et al. High fat diet
417 blunts stress-induced hypophagia and activation of Glp1r dorsal lateral septum neurons in male
418 but not in female mice. Molecular Metabolism. 2022;64:101571.

419 33. Terrill SJ, Holt MK, Maske CB, Abrams N, Reimann F, Trapp S, et al. Endogenous GLP-1 in
420 lateral septum promotes satiety and suppresses motivation for food in mice. Physiology &
421 Behavior. 2019;206:191-9.

422 34. Li S-B, Borniger JC, Yamaguchi H, Hédou J, Gaudilliere B, de Lecea L. Hypothalamic
423 circuitry underlying stress-induced insomnia and peripheral immunosuppression. Science
424 Advances.6(37):eabc2590.

425 35. Weninger SC, Muglia LJ, Jacobson L, Majzoub JA. CRH-deficient mice have a normal
426 anorectic response to chronic stress. Regul Pept. 1999;84(1-3):69-74.

427 36. Weninger SC, Dunn AJ, Muglia LJ, Dikkes P, Miczek KA, Swiergiel AH, et al. Stress-induced
428 behaviors require the corticotropin-releasing hormone (CRH) receptor, but not CRH.
429 Proceedings of the National Academy of Sciences. 1999;96(14):8283-8.

430 37. Muglia L, Jacobson L, Dikkes P, Majzoub JA. Corticotropin-releasing hormone deficiency
431 reveals major fetal but not adult glucocorticoid need. Nature. 1995;373(6513):427-32.

432 38. Dunn AJ, Swiergiel AH. Behavioral responses to stress are intact in CRF-deficient mice.
433 Brain Research. 1999;845(1):14-20.

434 39. Foster MT, Song CK, Bartness TJ. Hypothalamic paraventricular nucleus lesion involvement
435 in the sympathetic control of lipid mobilization. Obesity (Silver Spring). 2010;18(4):682-9.

436 40. Chen CR, Zhong YH, Jiang S, Xu W, Xiao L, Wang Z, et al. Dysfunctions of the
437 paraventricular hypothalamic nucleus induce hypersomnia in mice. Elife. 2021;10.

438 41. Kim ER, Xu Y, Cassidy RM, Lu Y, Yang Y, Tian J, et al. Paraventricular hypothalamus
439 mediates diurnal rhythm of metabolism. Nat Commun. 2020;11(1):3794.

440 42. Burmeister MA, Ayala JE, Smouse H, Landivar-Rocha A, Brown JD, Drucker DJ, et al. The
441 Hypothalamic Glucagon-Like Peptide 1 Receptor Is Sufficient but Not Necessary for the
442 Regulation of Energy Balance and Glucose Homeostasis in Mice. Diabetes. 2017;66(2):372-84.

443 43. Bozadjieva-Kramer N, Ross RA, Johnson DQ, Fenselau H, Haggerty DL, Atwood B, et al.
444 The Role of Mediobasal Hypothalamic PACAP in the Control of Body Weight and Metabolism.
445 Endocrinology. 2021;162(4).

446 44. Lee CM, Zhou L, Liu J, Shi J, Geng Y, Liu M, et al. Single-cell RNA-seq analysis revealed
447 long-lasting adverse effects of tamoxifen on neurogenesis in prenatal and adult brains. Proc
448 Natl Acad Sci U S A. 2020;117(32):19578-89.
449

450 **FIGURES AND FIGURE LEGENDS**

451 **Figure 1. AAV-Cre administration in PVN of *Crh*$^{f/f}$ mice results in the development of**
452 **metabolic syndrome. (A)** Experimental paradigm for virus delivery. AAV-Cre or AAV-eGFP was
453 stereotactically injected into the adult murine PVN. **(B)** Plasma corticosterone decreased following
454 AAV-Cre injection ($t(12) = 4.011$, $p = 0.0017$). **(C)** Changes in body weight following virus delivery
455 at week 0 (two-way ANOVA, main effect of Group: $F(1, 12) = 294.1$, $p < 0.0001$; main effect of
456 Time: $F(1.378, 16.53) = 228.5$, $p < 0.0001$; interaction between Group and Time: $F(9, 108) =$
457 138.4, $p < 0.0001$). **(D)** Daily chow intake following virus injection increased with AAV-Cre ($t(12)$
458 $= 3.152$, $p = 0.0083$). **(E)** Changes in oxygen consumption were observed over the course of 96
459 hours. **(F)** Quantification of the decrease in oxygen consumption in AAV-Cre-injected mice (two-
460 way ANOVA with Bonferroni's multiple comparisons test, main effect of Group: $F(1, 12) = 25.11$,
461 $p = 0.0003$; main effect of Time: $F(1, 12) = 208.4$, $p < 0.0001$; interaction between Group and
462 Time: $F(1, 12) = 43.58$, $p < 0.001$). **(G)** The respiratory exchange ratio (RER) was unaltered (two-
463 way ANOVA, no main effect of Group: $F(1, 12) = 0.02021$, $p = 0.8893$; no main effect of Time: F
464 $(1, 12) = 2.970$, $p = 0.1105$; no interaction between Group and Time: $F(1, 12) = 3.566$, $p = 0.0834$).
465 **(H)** Energy expenditure decreased following AAV-Cre delivery (two-way ANOVA with Bonferroni's
466 multiple comparisons test, main effect of Group: $F(1, 12) = 26.31$, $p = 0.0002$; main effect of Time:
467 $F(1, 12) = 207.9$, $p < 0.0001$; interaction between Group and Time: $F(1, 12) = 45.10$, $p < 0.0001$).
468 **(I)** Locomotion in the x-axis in the CLAMS cage decreased during the dark cycle (two-way ANOVA
469 with Bonferroni's multiple comparisons test, main effect of Group: $F(1, 12) = 8.461$, $p = 0.0131$;
470 main effect of Time: $F(1, 12) = 41.86$, $p < 0.0001$, interaction between Group and Time: $F(1, 12)$
471 $= 10.17$, $p = 0.0078$). **(J)** Proportion of fat mass as determined by EchoMRI increased in AAV-
472 Cre-injected mice ($t(12) = 12.67$, $p < 0.0001$). **(K)** Changes in average blood glucose after
473 overnight fasting ($t(12) = 5.888$, $p < 0.0001$). **(L)** The glucose tolerance test reveals increased
474 baseline blood glucose levels (two-way ANOVA with Bonferroni's multiple comparisons test, main
475 effect of Group: $F(1, 12) = 22.30$, $p = 0.0005$; main effect of Time: $F(2.717, 32.60) = 24.72$, $p <$
476 0.0001; interaction between Group and Time: $F(4, 48) = 3.111$, $p = 0.0235$). **(M)** The insulin
477 tolerance test reveals insulin tolerance (two-way ANOVA with Bonferroni's multiple comparisons
478 test, main effect of Group: $F(1, 11) = 11.30$, $p = 0.0063$; main effect of Time: $F(1.712, 18.84) =$
479 55.72, $p < 0.0001$; no interaction between Group and Time: $F(2, 22) = 0.6622$, $p = 0.5257$).
480 Sample sizes are as shown on graphs ($n = 7$ mice per group). Data are presented as individual
481 points and mean ± or + SEM.

482 **Figure 2. AAV-Cre action in PVN of *Crh*$^{f/f}$ mice depletes CRH and OXT. (A)** Example
483 comparison of CRH expression in PVN between both groups. **(B)** Example of OXT expression in
484 PVN. **(C)** CRH-positive cell density decreased following AAV-Cre expression in *Crh*$^{f/f}$ PVN (t (4) =
485 3.176, p = 0.0337). **(D)** OXT-positive cell density decreased as well (t (4) = 2.807, p = 0.0236).
486 **(E)** Overall cell density trended toward a decline (t (4) = 2.511, p = 0.0660). Sample sizes are as
487 shown on graphs (n = 3 mice per group). Data are presented as individual points and mean +
488 SEM.

489 **Figure 3: AAV-Cre action in wild-type PVN induces metabolic changes, neuronal cell death,**
490 **and recruitment of glia. (A)** Experimental paradigm for virus delivery in wild-type mice. **(B)**
491 Plasma corticosterone levels decreased after AAV-Cre injection (t (7) = 3.260, p = 0.0139). **(C)**
492 Body weight changes followed virus delivery (two-way ANOVA, main effect of Group: F (1, 7) =
493 22.37, p = 0.0021; main effect of Time: F (1.134, 7.940) = 191.5, p < 0.0001; interaction between
494 Group and Time: F (6, 42) = 79.71, p < 0.0001). **(D)** Daily food intake increased in AAV-Cre-
495 injected mice (Mann-Whitney test, U = 0, p = 0.0159). **(E)** Example images of neuronal nuclei
496 (NeuN) across the PVN following injection in wild-type mice. **(F)** Quantification of neuron density
497 at different stereotactic coordinates: -0.34 (t (5) = 18.72, p < 0.0001), -0.58 (t (5) = 5.343, p =
498 0.0031), -0.94 (t (5) = 3.053, p = 0.0283), and -1.22 (t (5) = 3.372, p = 0.0199). **(G)** Example
499 comparison of glial fibrillary acidic protein (GFAP) and ionized calcium binding adaptor molecule
500 1 (Iba1) expression in the wild-type PVN between the two groups. **(H)** Expression of astrocytes
501 increased as quantified by GFAP fluorescence area (t (6) = 3.017, p = 0.0235) **(I)** Expression of
502 microglia increased as quantified by Iba1 fluorescence area (t (6) = 2.917, p = 0.0267). Sample
503 sizes are as shown on graph: **(F)** n = 3 control, 4 AAV-Cre **(H, I)** n = 4 per group. Data are
504 presented as individual points and mean ± or + SEM.

505 **SUPPLEMENTARY INFORMATION**

506 **Figure S1: AAV-Cre expression in the PVN of female *Crh$^{f/f}$* mice recapitulates body weight**
507 **increases. (A)** Experimental paradigm for virus delivery. **(B)** Body weight increases following
508 AAV-Cre injection (two-way ANOVA, main effect of Group: $F(1, 4) = 59.08$, $p = 0.0015$; main effect
509 of Time: $F(1.782, 7.129) = 77.74$, $p < 0.0001$; interaction between Group and Time: $F(6, 24) =$
510 58.41, $p < 0.0001$). Sample sizes are as shown on graphs (n = 3 mice per group). Data are
511 presented as mean ± SEM.

512 **Figure S2: *Crh$^{f/f}$* mice expressing AAV-Cre in PVN display elevated anxiety-like behaviors.**
513 **(A)** Representative trajectories of AAV-GFP- (top) and AAV-Cre-injected (bottom) mice during the
514 open field test. **(B)** AAV-Cre-injected mice spent less time in the center zone of the open field test
515 ($t(12) = 2.181$, $p = 0.0498$), and changes in distance traveled were not significant ($t(12) = 1.811$,
516 $p = 0.0952$) during the open field test. **(C)** Representative trajectories of both groups during the
517 light-dark box test. **(D)** Time spent in the dark zone increased ($t(12) = 2.416$, $p = 0.0326$), and
518 entries into the light zone decreased (Mann-Whitney test, $U = 0$, $p = 0.0006$) during the light-dark
519 box test. Sample sizes are as shown on graphs (n = 7 mice per group). Data are presented as
520 individual points and mean + SEM.

521 **Figure S3. Wild-type mice injected with AAV-Cre in PVN exhibit increased anxiety-like**
522 **behaviors. (A)** Representative traces of wild-type mice during the open field test. **(B)** During the
523 open field test, time spent in the center zone decreased ($t(7) = 2.817$, $p = 0.0259$), and total
524 distance traveled decreased ($t(7) = 3.275$, $p = 0.0136$). **(C)** Representative movement during the
525 light-dark box test for both groups. **(D)** During the light-dark box test, time spent in the dark zone
526 increased ($t(7) = 2.798$, $p = 0.0266$), and entries into the light zone decreased ($t(7) = 3.142$, $p =$
527 0.0163). Sample sizes are as shown on graphs (n = 5 AAV-GFP-injected mice, n = 4 AAV-Cre-
528 injected mice). Data are presented as individual points and mean + SEM.

529 **Figure S4. AAV-Cre expression in the dLS of male *Glp1r$^{f/f}$* mice results in cell death without**
530 **metabolic deficits. (A)** Experimental paradigm for virus delivery. **(B)** Body weight was
531 unchanged (two-way ANOVA, main effect of Group: $F(1, 16) = 0.07282$, $p = 0.7907$; main effect
532 of Time: $F(1.826, 29.22) = 364.6$, $p < 0.0001$; interaction between Group and Time: $F(4, 64) =$
533 3.406, $p = 0.0138$). **(C)** Representative images of neuronal nuclei in the dLS after AAV-GFP or
534 AAV-Cre injection. **(D)** Neuron density decreased in the dLS after AAV-Cre expression ($t(4) =$
535 4.631, $p = 0.0098$). Sample sizes are as shown on graphs: **(B)** n = 9 mice per group; **(D)** n = 3
536 mice per group. Data are presented as individual points and mean ± or + SEM.

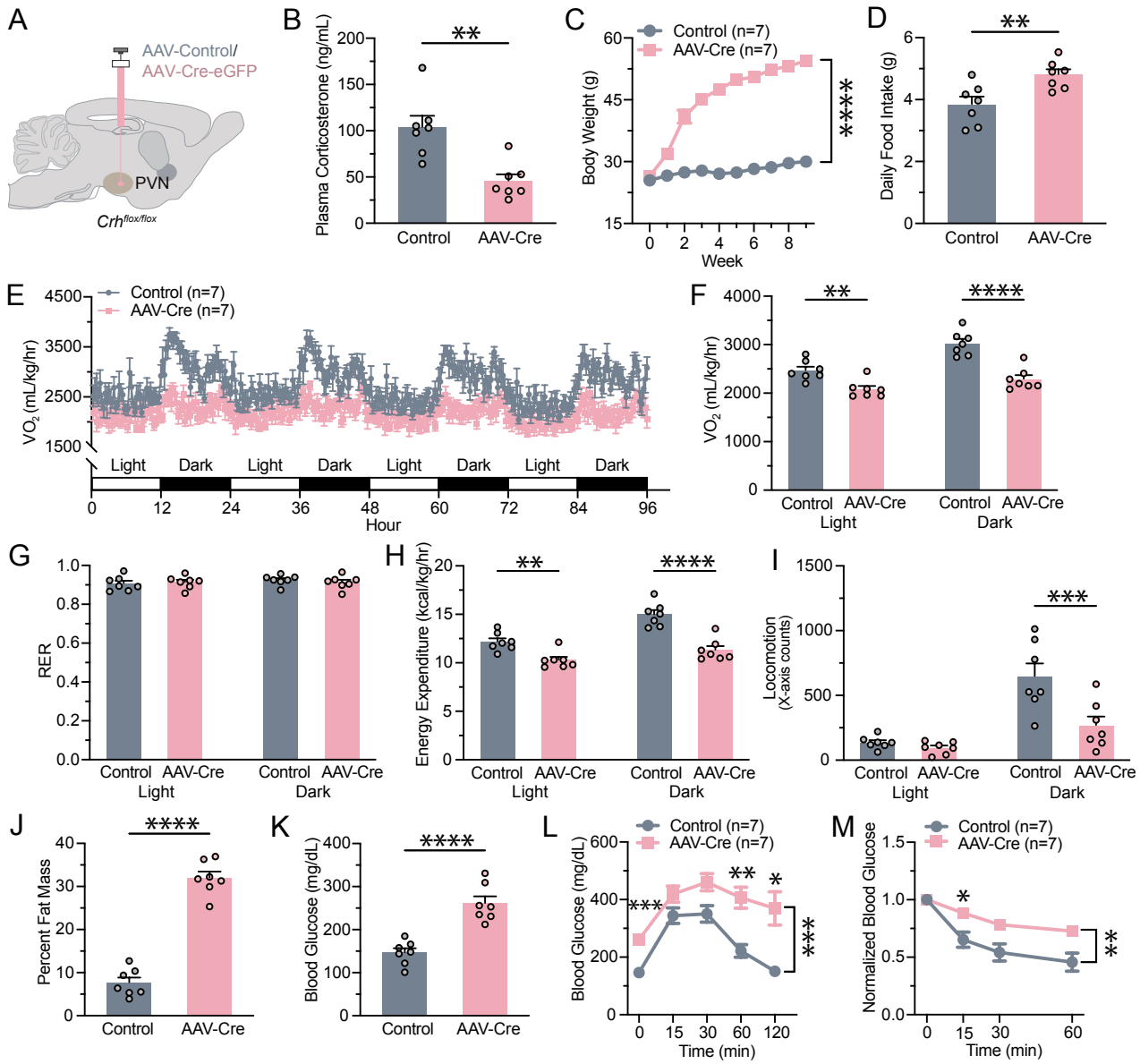

Savani et al. Figure 1

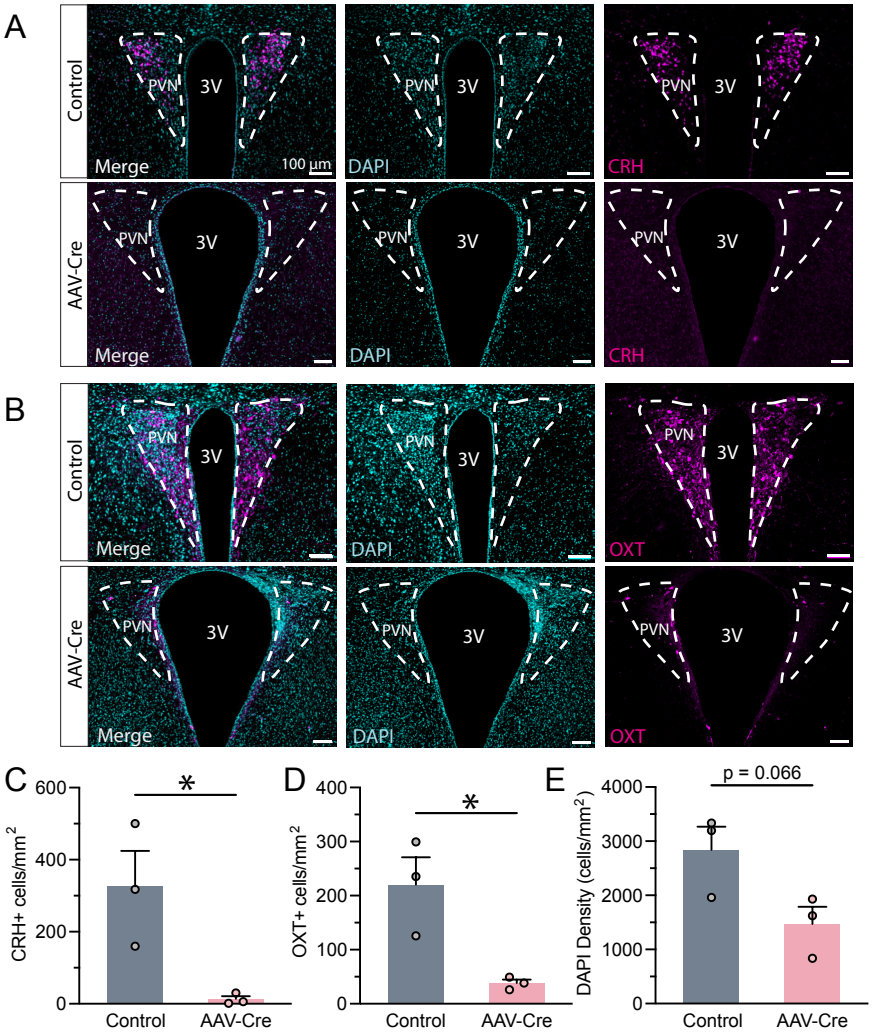

Savani et al. Figure 2

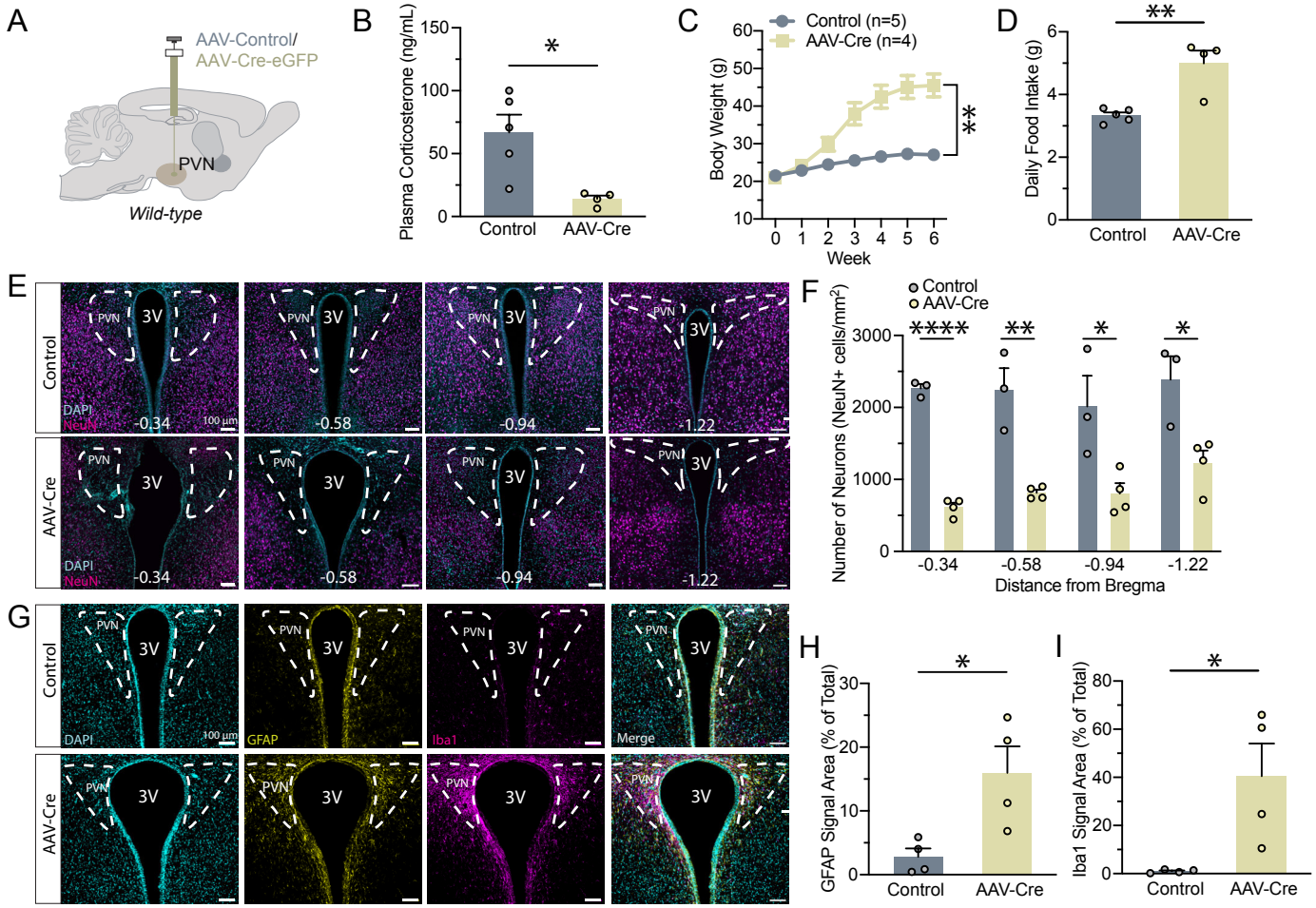

Savani et al. Figure 3

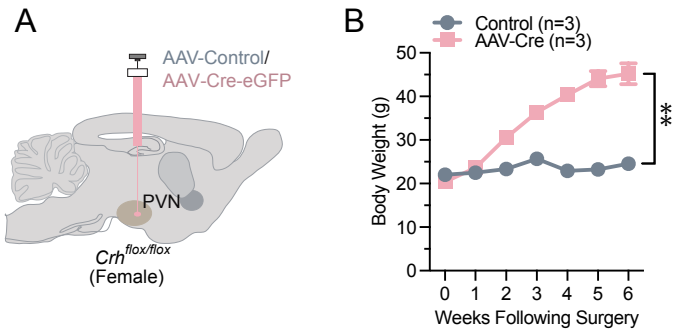

Savani et al. Supplementary Figure 1

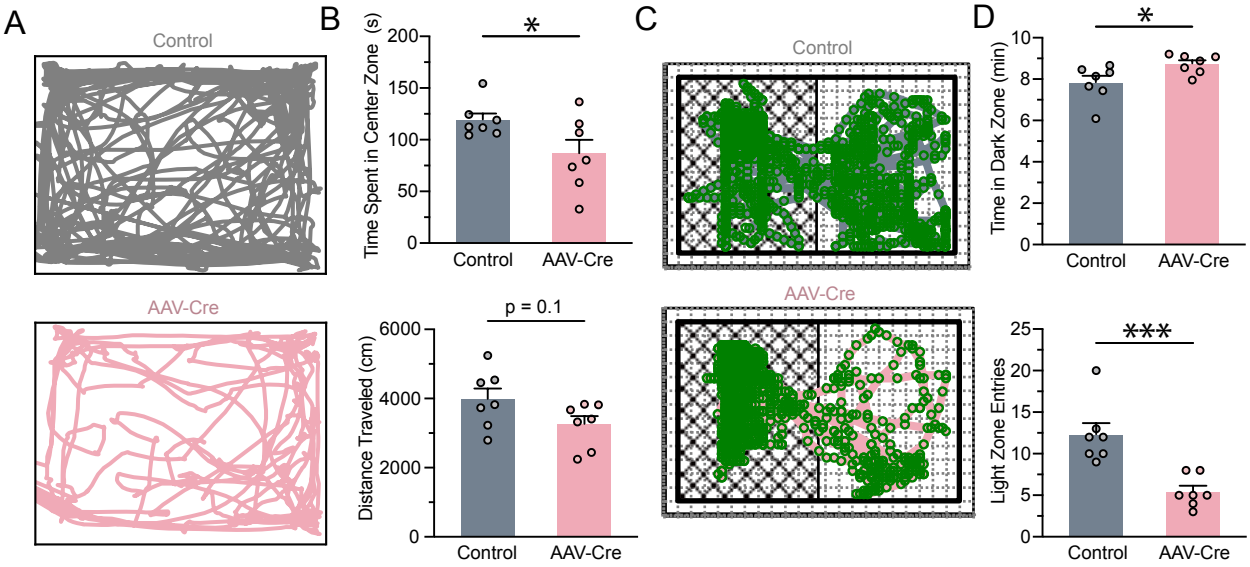

Savani et al. Supplementary Figure 2

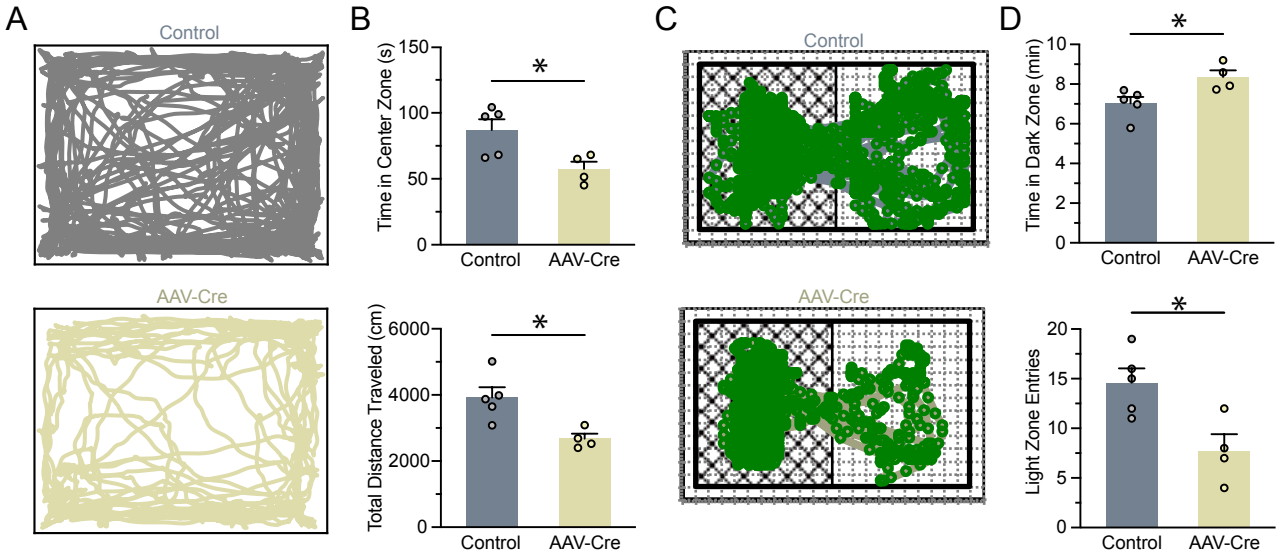

Savani et al. Supplementary Figure 3

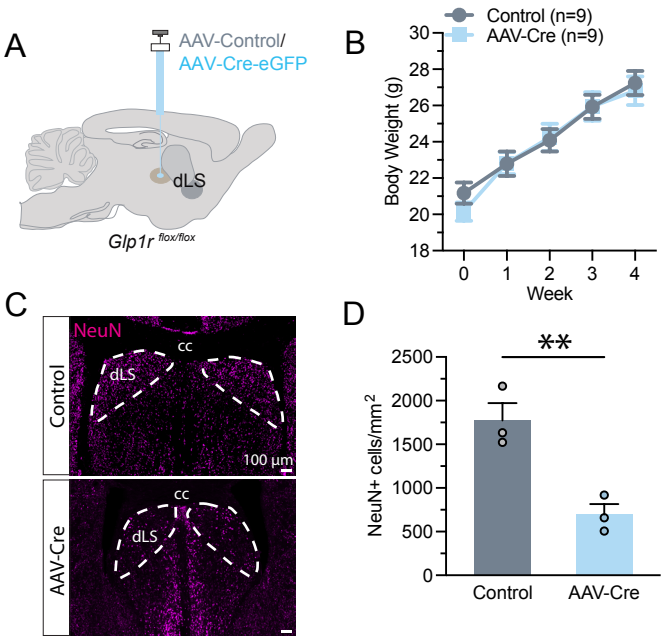

Savani et al. Supplementary Figure 4